

# An Effective Model of the Retinoic Acid Induced HL-60 Differentiation Program

Ryan Tasseff, Holly A. Jensen, Johanna Congleton<sup>†</sup>, Wei Dai, Andrew Yen<sup>†</sup>, and Jeffrey D. Varner\*

Robert Frederick Smith School of Chemical and Biomolecular Engineering and <sup>†</sup>Department of Biomedical Sciences, Cornell University, Ithaca NY 14853

**Running Title:** Effective modeling of HL-60 differentiation

**To be submitted:** *Frontiers in Systems Biology*

\*Corresponding author:

Jeffrey D. Varner,

Professor, Robert Frederick Smith School of Chemical and Biomolecular Engineering,  
244 Olin Hall, Cornell University, Ithaca NY, 14853

Email: jdv27@cornell.edu

Phone: (607) 255 - 4258

Fax: (607) 255 - 9166

## **Abstract**

In this study, we present an effective model All-Trans Retinoic Acid (ATRA)-induced differentiation of HL-60 cells. The model describes a key architectural feature of ATRA-induced differentiation, positive feedback between an ATRA-inducible signalsome complex involving many proteins including Vav1, a guanine nucleotide exchange factor, and the activation of the mitogen activated protein kinase (MAPK) cascade. The model, which was developed by integrating logical rules with kinetic modeling, was significantly smaller than previous models. However, despite its simplicity, it captured key features of ATRA induced differentiation of HL-60 cells. We identified an ensemble of effective model parameters using measurements taken from ATRA-induced HL-60 cells. Using these parameters, model analysis predicted that MAPK activation was bistable as a function of ATRA exposure. Conformational experiments supported ATRA-induced bistability. These findings, combined with other literature evidence, suggest that positive feedback is central to a diversity of cell fate programs.

## **1 Introduction**

2 Understanding differentiation programs is an important therapeutic challenge. Toward  
3 this challenge, lessons learned in model systems, such as the lineage-uncommitted hu-  
4 man myeloblastic cell line HL-60, informs our analysis of more complex therapeutically  
5 important programs. Patient derived HL-60 leukemia cells have been a durable experi-  
6 mental model since the 1970's (1). HL-60 undergoes cell cycle arrest and either myeloid  
7 or monocytic differentiation following stimulation; All-Trans Retinoic Acid (ATRA) induces  
8 G1/G0-arrest and myeloid differentiation in HL-60 cells, while 1,25-dihydroxy vitamin D3  
9 (D3) induces arrest and monocytic differentiation. Commitment to cell cycle arrest and dif-  
10 ferentiation requires approximately 48 hr of treatment, during which HL-60 cells undergo  
11 two division cycles.

12 Sustained mitogen-activated protein kinase (MAPK) activation is a defining feature of  
13 ATRA-induced HL-60 differentiation. ATRA drives sustained MEK-dependent activation of  
14 the RAF/MEK/ERK pathway, leading to arrest and differentiation (2). MEK inhibition re-  
15 sults in the loss of ERK and RAF phosphorylation, and the failure to arrest and differentiate  
16 (3). ATRA (and its metabolites) are ligands for the hormone activated nuclear transcrip-  
17 tion factors retinoic acid receptor (RAR) and retinoid X receptor (RXR) (4). RAR/RXR  
18 activation is necessary for ATRA-induced RAF phosphorylation (3), and the formation of  
19 the ATRA-inducible signalsome complex which drives differentiation. The signalsome is  
20 composed of Src family kinases Fgr and Lyn, PI3K, c-Cbl, Slp76, and KSR, as well as  
21 IRF-1 transcription factors (5–9). This signaling is driven by ATRA-induced expression of  
22 CD38 and the putative heterotrimeric Gq protein-coupled receptor BLR1 (10, 11). BLR1,  
23 identified as an early ATRA (or D3)-inducible gene using differential display (12), is neces-  
24 sary for MAPK activation and differentiation (11). Studies of the BLR1 promoter identified  
25 a 5' 17bp GT box approximately 1 kb upstream of the transcriptional start that conferred  
26 ATRA responsiveness (11). Members of the BLR1 transcriptional activator complex, e.g.

27 NFATc3 and CREB, are phosphorylated by ERK, JNK or p38 MAPK family members  
28 suggesting positive feedback between the signalsome and MAPK activation (13). BLR1  
29 overexpression enhanced RAF phosphorylation and accelerated terminal differentiation,  
30 while RAF inhibition reduced BLR1 expression and differentiation (14). BLR1 knock-out  
31 cells failed to activate RAF or differentiate in the presence of ATRA (14). Interestingly,  
32 both the knockdown or inhibition of Raf, also reduced BLR1 expression and functional dif-  
33 ferentiation (14). A recent computational study of ATRA-induced differentiation in HL-60  
34 cells suggested that the BLR1-MAPK positive feedback circuit was sufficient to explain  
35 ATRA-induced sustained MAPK activation and the expression of differentiation markers  
36 (15). Model analysis also suggested that Raf was the most distinct of the MAPK proteins.

37 A critical question is what other components of the MAPK positive feedback circuit are  
38 required to drive ATRA-induced functional differentiation of HL-60 cells. Wang and Yen  
39 showed that ectopic expression of the constitutively active CR3 domain of Raf1 restored  
40 ATRA-induced G0 arrest and differentiation in BLR1 knock-out cells (14). However, ec-  
41 topic expression of Raf1 CR3 alone, in the absence of ATRA, failed to induce arrest or  
42 differentiation. Thus, additional ATRA-inducible components must exist, which indepen-  
43 dently promote arrest and differentiation in the absence of BLR1. In this study, we devel-  
44 oped a mathematical model of the key architectural feature of ATRA induced differentiation  
45 of HL-60 cells, namely positive feedback between an ATRA-inducible signalsome complex  
46 and MAPK activation. Previously Tasseff et al. hypothesized that signalsome-MAPK posi-  
47 tive feedback was essential for ATRA-induced cell cycle arrest and differentiation (15). We  
48 explored this hypothesis by constructing a minimal model containing only signalsome and  
49 MAPK components (Fig. 2A). The effective model was developed using a novel frame-  
50 work which integrated logical rules with kinetic modeling. This formulation significantly  
51 reduced the size of the model compared to the previous study of Tasseff et al., while  
52 maintaining similar model performance (15). The effective model, despite its simplicity,

53 captured key features of ATRA induced differentiation of HL-60 cells. We identified an  
54 ensemble of effective model parameters using measurements taken from ATRA-induced  
55 HL-60 cells. Using these parameters, model analysis predicted the bistability of MAPK  
56 activation as a function of ATRA exposure. Conformational experiments supported ATRA-  
57 induced bistability. These findings, combined with other literature evidence, suggests that  
58 positive feedback architectures are central to many cell fate programs.

59 **Results**

60 Interrogation of the Raf interactome suggested Vav1 was involved with ATRA-induced  
61 initiation of MAPK activity (Fig. 1). The architecture ultimately responsible for mediating  
62 ATRA-induced Raf activation is not clear. To explore this question, we conducted immuno-  
63 precipitation and subsequent Western blotting to identify physical interactions between  
64 Raf and 19 putative interaction partners. A panel of 19 possible Raf interaction partners  
65 (kinases, GTPases, scaffolding proteins etc) was constructed based upon known signal-  
66 ing pathways. We did not consider the most likely binding partner, the small GTPase  
67 RAS, as previous studies have ruled it out in MAPK activation in HL-60 cells (14, 16).  
68 Total Raf was used as a bait protein for the immunoprecipitation studies. Western blot  
69 analysis using total Raf and pS621 Raf specific antibodies confirmed the presence of the  
70 bait protein, total and phosphorylated forms, in the immunoprecipitate (Fig. 1A). Of the  
71 19 proteins sampled, Vav1, Src, CK2, Akt, and 14-3-3 precipitated with Raf, suggesting a  
72 direct physical interaction was possible. However, only the associations between Raf and  
73 Vav1 and Raf and Src were ATRA-inducible (Fig. 1). Furthermore, the Vav1 and Src as-  
74 sociations were correlated with pS621 Raf abundance in the precipitate. Others proteins  
75 e.g., CK2, Akt and 14-3-3, generally bound Raf regardless of phosphorylation status or  
76 ATRA treatment. The remaining 14 proteins were expressed in whole cell lysate (Fig. 1B),  
77 but were not detectable in the precipitate of Raf IP. Treatment with the Raf kinase inhibitor  
78 GW5074 following ATRA exposure reduced the association of both Vav1 with Raf and  
79 Src with Raf (Fig. 1), although the signal intensity for Src was notably weak. However,  
80 GW5074 did not influence the association of CK2 or 14-3-3 with Raf, further demonstrat-  
81 ing their independence from Raf phosphorylation. Interestingly, the Raf-Akt interaction  
82 qualitatively increased following treatment with GW5074; however, it remained unaffected  
83 by treatment with ATRA. Src family kinases are known to be important in myeloid differ-  
84 entiation (17) and their role in HL-60 differentiation has been investigated elsewhere (5).

Given the existing work and variable reproducibility in the context of the Raf immunoprecipitate, we will not investigate the role of Src further in this study. Taken together, the immunoprecipitation and GW5074 results implicated Vav1 association to be correlated with Raf activation following ATRA-treatment. Previous studies demonstrated that a Vav1-Slp76-Cbl-CD38 complex plays an important role in ATRA-induced MAPK activation and differentiation of HL-60 cells (7). Here we did not observe direct interaction of Raf with Cbl or Slp76; however, this complex could be involved upstream.

Inhibition of Raf kinase activity modulated MAPK activation and differentiation markers following ATRA exposure (Fig. 1D-F). Next, we considered the effect of the Raf kinase inhibitor GW5074 on functional markers of ATRA-induced growth arrest and differentiation. ATRA treatment alone statistically significantly increased the G1/G0 percentage over the untreated control, while GW5074 alone had a negligible effect on the cell cycle distribution (Fig. 1D). Surprisingly, the combination of GW5074 and ATRA statistically significantly increased the G1/G0 population ( $82 \pm 1\%$ ) compared with ATRA alone ( $61 \pm 0.5\%$ ). Increased G1/G0 arrest following the combined treatment with GW5074 and ATRA was unexpected, as the combination of ATRA and the MEK inhibitor (PD98059) has been shown previously to decrease ATRA-induced growth arrest (2). However, growth arrest is not the sole indication of functional differentiation. Expression of the cell surface marker CD11b has also been shown to coincide with HL-60 cells myeloid differentiation (18). We measured CD11b expression, for the various treatment groups, using immunofluorescence flow cytometry 48 hr post-treatment. As with G1/G0 arrest, ATRA alone increased CD11b expression over the untreated control, while GW5074 further enhanced ATRA-induced CD11b expression (Fig. 1E). GW5074 alone had no statistically significant effect on CD11b expression, compared with the untreated control. Lastly, the inducible reactive oxygen species (ROS) response was used as a functional marker of differentiated neutrophils (10). We measured the ROS response induced by the phorbol ester 12-O-

111 tetradecanoylphorbol-13-acetate (TPA) using flow cytometry. Untreated cells showed no  
112 discernible TPA response, with only  $7.0 \pm 3.0\%$  ROS induction (Fig. 1F). Cells treated  
113 with ATRA had a significantly increased TPA response,  $53 \pm 7\%$  ROS induction 48 hr  
114 post-treatment. Treatment with both ATRA and GW5074 statistically significantly reduced  
115 ROS induction ( $22 \pm 0.6\%$ ) compared to ATRA alone. Interestingly, Western blot analy-  
116 sis did not detect a GW5074 effect on ATRA-induced expression of p47phox, a required  
117 upstream component of the ROS response (Fig. 1F, bottom). Thus, the inhibitory effect  
118 of GW5074 on inducible ROS might occur downstream of p47phox expression. How-  
119 ever, the ROS producing complex is MAPK dependent, therefore it is also possible that  
120 GW5074 inhibited ROS production by interfering with MAPK activation (in which case the  
121 p47Phox marker might not accurately reflect phenotypic conversion and differentiation).

122 We constructed an effective model of the ATRA-induced HL-60 differentiation circuit  
123 which described signaling and gene expression events following the addition of ATRA  
124 (Fig. 2). The model connectivity was developed from literature and the studies presented  
125 here. The signaling model recapitulated sustained signalsome/MAPK activation following  
126 exposure to  $1\mu\text{M}$  ATRA (Fig. 3A-B). An ensemble of effective model parameters was es-  
127 timated by minimizing the difference between simulations and time-series measurements  
128 of BLR1 mRNA and cRAF-pS621 following the addition of  $1\mu\text{M}$  ATRA. We focused on the  
129 S621 phosphorylation site of cRAF since enhanced phosphorylation at this site is a defin-  
130 ing characteristic of sustained MAPK activation in HL-60. The effective model captured  
131 both ATRA-induced BLR1 expression (Fig. 3A) and sustained phosphorylation of cRAF-  
132 pS621 (Fig. 3B) in a growing population of HL-60 cells. However, the effective model  
133 failed to capture the decline of BLR1 message after 48 hr of ATRA exposure. Next, we  
134 tested the response of the signalsome/MAPK signaling model to different ATRA dosages.

135 The signalsome/MAPK signaling model was bistable with respect to ATRA induction  
136 (Fig. 3C-D). Nullcline analysis predicted two stable steady-states and a single unstable

state when ATRA was present below a critical threshold (Fig. 3C). In the lower stable state, neither the signalsome nor cRAF-pS621 were present (thus, the differentiation program was deactivated). However, at the high stable state, both the signalsome and cRAF-pS621 were present, allowing for sustained activation and differentiation. Interestingly, when ATRA was above a critical threshold, only the activated state was accessible (Fig. 3D). To test these findings, we first identified the ATRA threshold. We exposed HL-60 cells to different ATRA concentrations for 72 hr (Fig. 3E). Morphological changes associated with differentiation were visible for ATRA  $\geq 0.25 \mu\text{M}$ , suggesting the critical ATRA threshold was near this concentration. Next, we conducted washout ATRA washout experiments to determine if activated cells remained activated even in the absence of ATRA. HL-60 cells locked into an activated state remained activated following ATRA withdraw (Fig. 4). Sustained activation resulted from reinforcing feedback between the signalsome and the MAPK pathway. Thus, following activation, if we inhibited or removed elements from the effective circuit we expected the signalsome and MAPK signals to decay. We simulated ATRA induced activation in the presence of kinase inhibitors, and without key circuit elements. Consistent with experimental results using multiple MAPK inhibitors, ATRA activation in the presence of MAPK inhibitors lowered the steady-state value of signalsome (Fig. 4A). In the presence of BLR1, the signalsome and cRAF-pS621 signals were maintained following ATRA withdraw (Fig. 4B, blue). On the other hand, BLR1 deletion removed the ability of the circuit to maintain a sustained MAPK response following the withdraw of ATRA (Fig. 4B, gray). Lastly, washout experiments in which cells were exposed to  $1 \mu\text{M}$  ATRA for 24 hr, and then transferred to fresh media without ATRA, confirmed the persistence of the self sustaining activated state for up to 144 hr (Fig. 4C). Thus, these experiments and simulations confirmed that reinforcing positive feedback likely drives the ATRA-induced differentiation program. Next, we analyzed the ATRA-induced downstream gene expression program following signalsome and cRaf activation.

163 The reduced order gene expression model described signal integration and ATRA-  
164 induced gene expression events in wild-type HL-60 cells (Fig. 5). The signalsome-MAPK  
165 model produced two outputs, Trigger and cRAF-S621 which drove the downstream dif-  
166 ferentiation program. In particular, Trigger, which is a surrogate for the RAR $\alpha$ /RXR tran-  
167 scriptional complex, regulated the expression of the transcription factors CCATT/enhancer  
168 binding protein  $\alpha$  (C/EBP $\alpha$ ), PU.1, and EGR1. In turn, these transcription factors, in com-  
169 bination with cRaf-S621, regulated the expression of downstream phenotypic markers  
170 such as CD38, CD11b or P47Phox. We assembled the connectivity of the signal integra-  
171 tion program driven by Trigger, and the phenotypic program from literature (supplemental  
172 materials). We estimated the parameters of the signal integration and phenotype pro-  
173 grams from previous studies which contained both steady-state and dynamic measure-  
174 ments of transcription factor and phenotypic marker expression following the addition of  
175 ATRA [REFHERE]. The model simulations captured the time dependent expression of  
176 both CD38 and CD11b following the addition ATRA (Fig. 5A), and steady-state values for  
177 upstream members of the signal integration unit (Fig. 5B).

178 **Discussion**

179 In this study, we presented an effective model of ATRA-inducible differentiation of HL-60  
180 cells which encoded positive feedback between the ATRA-inducible signalsome complex  
181 and the MAPK pathway. Despite its simplicity, the model captured key features of the  
182 ATRA induced differentiation such as sustained MAPK activation, and bistability with re-  
183 spect to ATRA exposure. We also reported a new ATRA-inducible component of the sig-  
184 nalsome, Vav1. Vav1 is a guanine nucleotide exchange factor for Rho family GTPases that  
185 activate pathways leading to actin cytoskeletal rearrangements and transcriptional alter-  
186 ations (19). The Vav1/RAF association correlated with RAF activity, was ATRA-inducible  
187 and decreased after treatment with GW5074. The presence of Vav1 in RAF/Grb2 com-  
188 plexes has been shown to correlate with increased Raf activity in mast cells (20). Fur-  
189 thermore, studies on Vav1 knockout mice demonstrated that the loss of Vav1 resulted  
190 in deficiencies of ERK signaling for both T-cells as well as neutrophils (21, 22). While its  
191 function in the signalsome is unclear, Vav1 has been shown to associate with a Cbl-Slp76-  
192 CD38 complex in an ATRA-dependent manner; furthermore, transfection of HL-60 cells  
193 with Cbl mutants that fail to bind CD38, yet still bind Slp76 and Vav1, prevented ATRA-  
194 induced MAPK activation (7). Thus, interaction of Cbl-Slp76-Vav1 and CD38 appears to  
195 be required for transmission of the ATRA signal by the signalsome.

196 We conducted immunoprecipitation studies and identified a limited number of ATRA-  
197 dependent and -independent Raf interaction partners. While we were unable to detect  
198 the association of Raf with common kinases and GTPases such as PKC, PKA, p38, Rac  
199 and Rho, we did establish potential interactions between Raf and key partners such as  
200 Vav1, Src, Akt, CK2 and 14-3-3. All of these partners are known to be associated with Raf  
201 activation or function. Src is known to bind Raf through an SH2 domain, and this associ-  
202 ation has been shown to be dependent of the serine phosphorylation of Raf (23). Thus,  
203 an ATRA inducible Src/Raf association may be a result of ATRA-induced Raf phospho-

204 phosphorylation at S259 or S621. We also identified an interaction between Raf and the Ser/Thr  
205 kinases Akt and CK2. Akt can phosphorylate Raf at S259, as demonstrated by studies  
206 in a human breast cancer line (24). CK2 can also phosphorylate Raf, although the lit-  
207 erature has traditionally focused on S338 and not S621 or S259(25). However, neither  
208 of these kinase interactions were ATRA-inducible, suggesting their association with Raf  
209 alone was not associated with ATRA-induced Raf phosphorylation. The adapter protein  
210 14-3-3 was also constitutively associated with Raf. The interaction between Raf and 14-  
211 3-3 has been associated with both S621 and S259 phosphorylation and activity (26).  
212 Additionally, the association of Raf with 14-3-3 not only stabilized S621 phosphorylation,  
213 but also reversed the S621 phosphorylation from inhibitory to activating (27). Finally, we  
214 found that Vav1/Raf association correlated with Raf activity, was ATRA-inducible and de-  
215 creased after treatment with GW5074. The presence of Vav1 in Raf/Grb2 complexes has  
216 been shown to correlate with increased Raf activity in mast cells (20). Furthermore, stud-  
217 ies on Vav1 knockout mice demonstrated that the loss of Vav1 resulted in deficiencies of  
218 ERK signaling for both T-cells as well as neutrophils (21, 22). Interestingly, while an in-  
219 tegrin ligand-induced ROS response was blocked in Vav1 knockout neutrophils, TPA was  
220 able to bypass the Vav1 requirement and stimulate both ERK phosphorylation and ROS  
221 induction (22). In this study, the TPA-induced ROS response was dependent upon Raf  
222 kinase activity, and was mitigated by the addition of GW5074. It is possible that Vav1 is  
223 downstream of various integrin receptors but upstream of Raf in terms of inducible ROS  
224 responses. Vav1 has also been shown to associate with a Cbl-Slp76-CD38 complex in  
225 an ATRA-dependent manner; furthermore, transfection of HL-60 cells with Cbl mutants  
226 that fail to bind CD38, yet still bind Slp76 and Vav1, prevents ATRA-induced MAPK acti-  
227 vation (7). The literature suggest a variety of possible receptor-signaling pathways, which  
228 involve Vav1, for MAPK activation; moreover, given the ATRA-inducible association Vav1  
229 may play a direct role in Raf activation.

230 We hypothesized that Vav1 is a member of an ATRA-inducible complex which propels  
231 sustained MAPK activation, arrest and differentiation. Initially, ATRA-induced Vav1 ex-  
232 pression drives increased association between Vav1 and Raf. This increased interaction  
233 facilitates phosphorylation and activation of Raf by pre-bound Akt and/or CK2 at S621  
234 or perhaps S259. Constitutively bound 14-3-3 may also stabilize the S621 phosphory-  
235 lation, modulate the activity and/or up-regulate autophosphorylation. Activated Raf can  
236 then drive ERK activation, which in turn closes the positive feedback loop by activating  
237 Raf transcription factors, e.g. Sp1 and/or STAT1 (28–31). We tested this working hy-  
238 pothesis using mathematical modeling. The model recapitulated both ATRA time-course  
239 data as well as the GW5074 inhibitor effects. This suggested the proposed Raf-Vav1  
240 architecture was at least consistent with the experimental studies. Further, analysis of  
241 the Raf-Vav1 model identified bistability in ppERK levels. Thus, two possible MAPK ac-  
242 tivation branches were possible for experimentally testable ATRA values. The analysis  
243 also suggested the ATRA-induced Raf-Vav1 architecture could be locked into a sustained  
244 signaling mode (high ppERK) even in the absence of a ATRA signal. This locked-in prop-  
245 erty could give rise to an ATRA-induction memory. We validated the treatment memory  
246 property predicted by the Raf-Vav1 circuit experimentally using ATRA-washout experi-  
247 ments. ERK phosphorylation levels remained high for more then 96 hr after ATRA was  
248 removed. Previous studies demonstrated that HL-60 cells possessed an inheritable mem-  
249 ory of ATRA stimulus (32). Although the active state was self-sustaining, the inactive state  
250 demonstrated considerable robustness to perturbation. For example, we found that 50x  
251 overexpression of Raf was required to reliably lock MAPK into the activated state, while  
252 small perturbations had almost no effect on ppERK levels over the entire ensemble. CD38  
253 expression correlated with the ppERK, suggesting its involvement in the signaling com-  
254 plex. Our computational and experimental results showed that positive feedback, through  
255 ERK-dependent Raf expression, could sustain MAPK signaling through many division cy-

256 cles. Such molecular mechanisms could underly aspects of cellular memory associated  
257 to consecutive ATRA treatments.

258 Several engineered, or naturally occurring systems involved in cell fate decisions incor-  
259 porate positive feedback and bistability (33). One of the most well studied cell fate circuits  
260 is the Mos mitogen-activated protein kinase cascade in *Xenopus* oocytes. This cascade  
261 is activated when oocytes are induced by the steroid hormone progesterone (34). The  
262 MEK-dependent activation of p42 MAPK stimulates the accumulation of the Mos onco-  
263 protein, which in turn activates MEK, thereby closing the feedback loop. This is similar to  
264 the differentiation circuit presented here; ATRA drives signalsome which activates MAPK,  
265 cell-cycle arrest, differentiation and signalsome. Thus, while HL-60 and *Xenopus* oocytes  
266 are vastly different biological models, they share similar cell fate decision architectures.  
267 Other unrelated cell fate decisions such as programmed cell death have also been sug-  
268 gested to be bistable (35). Still more biochemical networks important to human health,  
269 for example the human coagulation or complement cascades, also feature strong positive  
270 feedback elements (36). Thus, while positive feedback is sometimes not desirable in man-  
271 made systems, it may be at the core of a diverse variety of cell fate programs and other  
272 networks important to human health.

273 Model performance was impressive given its limited size. However, there were sev-  
274 eral issues to explore further. First, there was likely missing connectivity in the effective  
275 differentiation circuit. Decreasing BLR1 expression with simultaneously sustained cRAF-  
276 pS261 activation was not captured by the current network architecture. This suggested  
277 that signalsome, once activated, had a long lifetime as decreased BLR1 expression did  
278 not impact cRAF-pS261 abundance. We could model this by separating signalsome for-  
279 mation into an inactive precursor pool that is transformed to a long-lived activated siganlsome  
280 by MAPK activation. We should also explore adding additional downstream bio-  
281 logical modules to this skeleton model, for example the upregulation of reactive oxygen

282 markers such as p47Phox or cell cycle arrest components to capture the switch from an  
283 actively proliferating population to a population in G0-arrest. Next, the choice of max/min  
284 integration rules or the particular form of the transfer functions could also be explored.  
285 Integration rules other than max/min could be used, such as the mean or the product, as-  
286 suming the range of the transfer functions is always  $f \in [0, 1]$ . Alternative integration rules  
287 might have different properties which could influence model identification or performance.  
288 For example, a mean integration rule would be differentiable, allowing derivative-based  
289 optimization approaches to be used. The form of the transfer function could also be ex-  
290 plored. We choose hill-like functions because of their prominence in the systems and  
291 synthetic biology community. However, many other transfer functions are possible.

292 **Materials and Methods**

293 *Effective ATRA differentiation model.* ATRA induced signaling events were modeled us-  
 294 ing saturation kinetics within an ordinary differential equation (ODE) framework:

$$\frac{1}{\tau_i} \frac{dx_i}{dt} = \sum_{j=1}^{\mathcal{R}} \sigma_{ij} r_j(\mathbf{x}, \epsilon, \mathbf{k}) - (\mu + k_d) x_i \quad i = 1, 2, \dots, \mathcal{M} \quad (1)$$

295 The quantity  $x_i$  denotes concentration of signaling species  $i$ , while  $\mathcal{R}$  and  $\mathcal{M}$  denote the  
 296 number of signaling reactions and signaling species in the model, respectively. The quan-  
 297 tity  $\tau_i$  denotes a time scale parameter for species  $i$  which captures un-modeled effects; in  
 298 the current study  $\tau_i = 1$  for all species. The quantity  $r_j(\mathbf{x}, \epsilon, \mathbf{k})$  denotes the rate of pro-  
 299 cess  $j$ . Typically, process  $j$  is a non-linear function of biochemical and enzyme species  
 300 abundance, as well as unknown model parameters  $\mathbf{k}$  ( $\mathcal{K} \times 1$ ). The quantity  $\sigma_{ij}$  denotes the  
 301 stoichiometric coefficient for species  $i$  in reaction  $j$ . If  $\sigma_{ij} > 0$ , species  $i$  is produced by  
 302 reaction  $j$ . Conversely, if  $\sigma_{ij} < 0$ , species  $i$  is consumed by reaction  $j$ , while  $\sigma_{ij} = 0$  indi-  
 303 cates species  $i$  is not connected with reaction  $j$ . Lastly,  $\mu$  denotes the specific growth rate,  
 304 and  $k_d$  denotes the rate constant controlling cell death. Species balances were subject to  
 305 the initial conditions  $\mathbf{x}(t_o) = \mathbf{x}_o$ .

306 Signaling rate processes were written as the product of a kinetic term ( $\bar{r}_j$ ) and a control  
 307 term ( $v_j$ ) in the HL-60 model. The rate of an enzyme catalyzed process was modeled  
 308 using saturation kinetics:

$$\bar{r}_j = k_j \epsilon_i \prod_{s \in m_j^-} \left( \frac{x_s}{K_{js} + x_s} \right) \quad (2)$$

309 where  $k_j$  denotes the catalytic rate constant for reaction  $j$ ,  $\epsilon_i$  denotes the abundance of the  
 310 enzyme catalyzing reaction  $j$ , and  $K_{js}$  denotes the saturation constant for species  $s$  and  
 311  $s \in m_j$  denotes the set of *reactants* for reaction  $j$ . The control terms  $0 \leq v_j \leq 1$  depended  
 312 upon the combination of factors which influenced rate process  $j$ . For each rate, we used

313 a rule-based approach to select from competing control factors. If rate  $j$  was influenced  
 314 by  $1, \dots, m$  factors, we modeled this relationship as  $v_j = \mathcal{I}_j(f_{1j}(\cdot), \dots, f_{mj}(\cdot))$  where  
 315  $0 \leq f_{ij}(\cdot) \leq 1$  denotes a regulatory transfer function quantifying the influence of factor  $i$   
 316 on rate  $j$ . The function  $\mathcal{I}_j(\cdot)$  is an integration rule which maps the output of regulatory  
 317 transfer functions into a control variable. In this study, we used  $\mathcal{I}_j \in \{\min, \max\}$  and hill  
 318 transfer functions (37). If a process had no modifying factors,  $v_j = 1$ .

319 The HL-60 model described both signal transduction and gene expression events fol-  
 320 lowing the addition of ATRA. The output of the signal transduction model was the input to  
 321 the gene expression model. For each gene  $j = 1, 2, \dots, \mathcal{G}$ , we modeled both the mRNA  
 322 ( $m_j$ ) and protein ( $p_j$ ):

$$\frac{dm_j}{dt} = r_{T,j} - (\mu + \theta_{m,j}) m_j + \lambda_j \quad (3)$$

$$\frac{dp_j}{dt} = r_{X,j} - (\mu + \theta_{p,j}) p_j \quad (4)$$

323 The terms  $r_{T,j}$  and  $r_{X,j}$  denote the specific rates of transcription, and translation while  
 324 the terms  $\theta_{m,j}$  and  $\theta_{p,j}$  denote first-order degradation constants for mRNA and protein,  
 325 respectively. The specific transcription rate was modeled as the product of a kinetic term  
 326  $\bar{r}_{T,j}$  and a control term  $u_j$  which described how the abundance of transcription factors, or  
 327 other regulators influenced the expression of gene  $j$ . The kinetic rate of transcription was  
 328 modeled as:

$$\bar{r}_{T,j} = V_T^{\max} \left( \frac{L_{T,o}}{L_{T,j}} \right) \left( \frac{G_j}{K_T + G_j} \right) \quad (5)$$

329 where the maximum gene expression rate  $V_T^{\max}$  was defined as the product of a char-  
 330 acteristic transcription rate constant ( $k_T$ ) and the abundance of RNA polymerase ( $R_1$ ),  
 331  $V_T^{\max} = k_T (R_1)$ . The  $(L_{T,o}/L_{T,j})$  term denotes the ratio of transcription read lengths,  
 332 where  $L_{T,o}$  is a characteristic gene length, and  $L_{T,j}$  denotes the length of gene  $j$ . Thus,  
 333 the  $(L_{T,o}/L_{T,j})$  term is gene specific correction to the characteristic transcription rate. The

<sup>334</sup> degradation rate constants were defined as  $\theta_{m,j}$  and  $\theta_{p,j}$  denote characteristic degradation  
<sup>335</sup> constants for mRNA and protein, respectively.

<sup>336</sup> The gene expression control term  $0 \leq u_j \leq 1$  depended upon the combination of  
<sup>337</sup> factors which influenced rate process  $j$ . If the expression of gene  $j$  was influenced  
<sup>338</sup> by  $1, \dots, m$  factors, we modeled this relationship as  $u_j = \mathcal{I}_j(f_{1j}(\cdot), \dots, f_{mj}(\cdot))$  where  
<sup>339</sup>  $0 \leq f_{ij}(\cdot) \leq 1$  denotes a regulatory transfer function quantifying the influence of factor  
<sup>340</sup>  $i$  on the expression of gene  $j$ , and  $\mathcal{I}_j(\cdot)$  denotes an integration rule. In this study, the  
<sup>341</sup> integration rule governing gene expression was the weighted fraction of promoter config-  
<sup>342</sup> urations resulting in gene expression. Thus, the control variable  $u_j$  took the form:

$$u_j = \frac{W_{R_{1,j}} + \sum_n W_{nj} f_{nj}}{1 + W_{R_{1,j}} + \sum_d W_{dj} f_{dj}} \quad (6)$$

<sup>343</sup> where the numerator, the weighted sum (with weights  $W_{nj}$ ) of promoter configurations  
<sup>344</sup> leading to gene expression, was normalized by all possible promoter configurations. The  
<sup>345</sup> likelihood of each configuration was quantified by the transfer function  $f_{nj}$  (which we mod-  
<sup>346</sup> eled using hill like functions), while the lead term in the numerator  $W_{R_{1,j}}$  denotes the  
<sup>347</sup> weight of constitutive expression for gene  $j$ . If a gene expression process had no modify-  
<sup>348</sup> ing factors,  $u_j = 1$ . Lastly, the specific translation rate was modeled as:

$$r_{X,j} = V_X^{\max} \left( \frac{m_j}{K_X + m_j} \right) \quad (7)$$

<sup>349</sup> where  $V_X^{\max}$  denotes a characteristic maximum translation rate estimated from literature,  
<sup>350</sup> and  $K_X$  denotes a translation saturation constant. The characteristic maximum translation  
<sup>351</sup> rate was defined as the product of a characteristic translation rate constant ( $k_X$ ) and the  
<sup>352</sup> Ribosome abundance ( $R_2$ ),  $V_X^{\max} = k_X (R_2)$ .

<sup>353</sup> In this study, we estimated the  $W_{ij}$  parameters, and the parameters in the trans-

354 fer functions  $f_{dj}$  from gene expression data sets. On the other hand, we estimated  
 355  $k_T, k_X, \theta_{m,j}, \theta_{p,j}, R_1$  and  $R_2$  using estimates of transcription and translation rates, the half-  
 356 life of a typical mRNA and protein, and a typical value for the copies per cell of RNA  
 357 polymerase and ribosomes from literature (38). The saturation constants  $K_X$  and  $K_T$   
 358 were adjusted so that gene expression and translation resulted in gene products on a bio-  
 359 logically realistic concentration scale. Lastly, we calculated the concentration for gene  $G_j$   
 360 by assuming, on average, that a cell had two copies of each gene at any given time. Thus,  
 361 the bulk of our gene expression parameters were based directly upon literature values,  
 362 and were not adjusted during model identification. The values used for the characteris-  
 363 tic transcription/translation parameters, degradation constants and macromolecular copy  
 364 number are given in the supplemental materials along with the specific formulas required  
 365 to calculate all derived constants.

366 *Estimation of signaling and gene expression model parameters.* Signal and gene ex-  
 367 pression model parameters were estimated by minimizing the squared difference between  
 368 simulations and experimental data set  $j$ :

$$E_j(\mathbf{k}) = \sum_{i=1}^{\mathcal{T}_j} \left( \hat{\mathcal{M}}_{ij} - \hat{y}_{ij}(\mathbf{k}) \right)^2 + \left( \frac{\mathcal{M}'_{ij} - \max y_{ij}}{\mathcal{M}'_{ij}} \right)^2 \quad (8)$$

369 The terms  $\hat{\mathcal{M}}_{ij}$  and  $\hat{y}_{ij}$  denote scaled experimental observations and simulation outputs  
 370 at time  $i$  from training set  $j$ , where  $\mathcal{T}_j$  denoted the number of time points for data set  $j$ .  
 371 The first term in Eqn. (8) quantified the relative simulation error. We used immunoblot  
 372 intensity measurements for model training. Thus, we trained the model on the *relative*  
 373 change between bands within each data set. Suppose we have the intensity of species  $x$   
 374 at time  $\{t_1, t_2, \dots, t_n\}$  in condition  $j$ . The scaled value  $0 \leq \hat{\mathcal{M}}_{ij} \leq 1$  is given by:

$$\hat{\mathcal{M}}_{ij} = \left( \mathcal{M}_{ij} - \min_i \mathcal{M}_{ij} \right) / \left( \max_i \mathcal{M}_{ij} - \min_i \mathcal{M}_{ij} \right) \quad (9)$$

375 where  $\hat{M}_{ij} = 0$  and  $\hat{M}_{ij} = 1$  describe the lowest (highest) intensity bands. A similar  
376 scaling was used for the simulation output. The second term in the objective function  
377 ensured a realistic concentration scale was estimated by the model. We set the highest  
378 intensity band to  $M'_{ij} = 10$  [AU] for all simulations. We minimized the total model residual  
379  $\sum_j E_j$  using heuristic optimization starting from a random initial parameter guess.

380 The signaling and gene expression model equations were implemented in Julia and  
381 solved using the CVODE routine of the Sundials package (39, 40). The model code and  
382 parameter ensemble is freely available under an MIT software license and can be down-  
383 loaded from <http://www.varnerlab.org>.

384 *Cell culture and treatment* Human myeloblastic leukemia cells (HL-60 cells) were grown  
385 in a humidified atmosphere of 5% CO<sub>2</sub> at 37°C and maintained in RPMI 1640 from Gibco  
386 (Carlsbad, CA) supplemented with 5% heat inactivated fetal bovine serum from Hyclone  
387 (Logan, UT) and 1× antibiotic/antimicotic (Gibco, Carlsbad, CA). Cells were cultured in  
388 constant exponential growth (41). Experimental cultures were initiated at  $0.1 \times 10^6$  cells/mL  
389 24 hr prior to ATRA treatment; if indicated, cells were also treated with GW5074 (2 $\mu$ M) 18  
390 hr before ATRA treatment. For the cell culture washout experiments, cells were treated  
391 with ATRA for 24 hr, washed 3x with prewarmed serum supplemented culture medium  
392 to remove ATRA, and reseeded in ATRA-free media as described. Western blot analysis  
393 was performed at incremental time points after removal of ATRA.

394 *Chemicals* All-Trans Retinoic Acid (ATRA) from Sigma-Aldrich (St. Louis, MO) was dis-  
395 solved in 100% ethanol with a stock concentration of 5mM, and used at a final concen-  
396 tration of 1 $\mu$ M (unless otherwise noted). The cRAF inhibitor GW5074 from Sigma-Aldrich  
397 (St. Louis, MO) was dissolved in DMSO with a stock concentration of 10mM, and used  
398 at a final concentration of 2 $\mu$ M. HL-60 cells were treated with 2 $\mu$ M GW5074 with or with-  
399 out ATRA (1 $\mu$ M) at 0 hr. This GW5074 dosage had a negligible effect on the cell cycle  
400 distribution, compared to ATRA treatment alone.

401 *Immunoprecipitation and western blotting* Approximately  $1.2 \times 10^7$  cells were lysed using  
402  $400\mu\text{L}$  of M-Per lysis buffer from Thermo Scientific (Waltham, MA). Lysates were cleared  
403 by centrifugation at  $16,950 \times g$  in a micro-centrifuge for 20 min at  $4^\circ\text{C}$ . Lysates were  
404 pre-cleared using  $100\mu\text{L}$  protein A/G Plus agarose beads from Santa Cruz Biotechnology  
405 (Santa Cruz, CA) by inverting overnight at  $4^\circ\text{C}$ . Beads were cleared by centrifugation and  
406 total protein concentration was determined by a BCA assay (Thermo Scientific, Waltham,  
407 MA). Immunoprecipitations were setup by bringing lysate to a concentration of 1g/L in a  
408 total volume of  $300\mu\text{L}$  (M-Per buffer was used for dilution). The anti-RAF antibody was  
409 added at  $3\mu\text{L}$ . A negative control with no bait protein was also used to exclude the di-  
410 rect interaction of proteins with the A/G beads. After 1 hr of inversion at  $4^\circ\text{C}$ ,  $20\mu\text{L}$  of  
411 agarose beads was added and samples were left to invert overnight at  $4^\circ\text{C}$ . Samples  
412 were then washed three times with M-Per buffer by centrifugation. Finally proteins were  
413 eluted from agarose beads using a laemmli loading buffer. Eluted proteins were resolved  
414 by SDS-PAGE and Western blotting. Total lysate samples were normalized by total protein  
415 concentration ( $20\mu\text{g}$  per sample) and resolved by SDS-PAGE and Western blotting. Sec-  
416 ondary HRP bound antibody was used for visualization. All antibodies were purchased  
417 from Cell Signaling (Boston, MA) with the exception of  $\alpha$ -p621 RAF which was purchased  
418 from Biosource/Invitrogen (Carlsbad, CA), and  $\alpha$ -CK2 from BD Biosciences (San Jose,  
419 CA).

420 *Morphology assessment* Untreated and ATRA-treated HL-60 cells were collected after  
421 72 hr and cytocentrifuged for 3 min at 700 rpm onto glass slides. Slides were air-dried  
422 and stained with Wright's stain. Slide images were captured at 40X (Leica DM LB 100T  
423 microscope, Leica Microsystems).

424 **Competing interests**

425 The authors declare that they have no competing interests.

426 **Author's contributions**

427 J.V and A.Y directed the study. R.T, H.J and J.C conducted the cell culture measure-  
428 ments. J.V and W.D developed the reduced order HL-60 models and the parameter en-  
429 semble. W.D analyzed the model ensemble, and generated figures for the manuscript.  
430 The manuscript was prepared and edited for publication by W.D, A.Y and J.V.

431 **Acknowledgements**

432 We gratefully acknowledge the suggestions from the anonymous reviewers to improve  
433 this manuscript.

434 **Funding**

435 We acknowledge the financial support to J.V. by the National Science Foundation CA-  
436 REER (CBET-0846876) for the support of R.T. and H.J. In addition, we acknowledge  
437 support to A.Y. from the National Institutes of Health (CA 30555, CA152870) and a grant  
438 from New York State Stem Cell Science. Lastly, we acknowledge the financial support to  
439 J.V. and A.Y. from the National Cancer Institute (#U54 CA143876). The content is solely  
440 the responsibility of the authors and does not necessarily represent the official views of  
441 the National Cancer Institute or the National Institutes of Health.

442 **References**

- 443 1. Breitman TR, Selonick SE, Collins SJ (1980) Induction of differentiation of the human  
444 promyelocytic leukemia cell line (HL-60) by retinoic acid. *Proc Natl Acad Sci U S A*  
445 77: 2936–2940.
- 446 2. Yen A, Roberson MS, Varvayanis S, Lee AT (1998) Retinoic acid induced  
447 mitogen-activated protein (MAP)/extracellular signal-regulated kinase (ERK) kinase-  
448 dependent MAP kinase activation needed to elicit HL-60 cell differentiation and  
449 growth arrest. *Cancer Res* 58: 3163–3172.
- 450 3. Hong HY, Varvayanis S, Yen A (2001) Retinoic acid causes MEK-dependent RAF  
451 phosphorylation through RARalpha plus RXR activation in HL-60 cells. *Differentiation*  
452 68: 55–66.
- 453 4. Mangelsdorf DJ, Ong ES, Dyck JA, Evans RM (1990) Nuclear receptor that identifies  
454 a novel retinoic acid response pathway. *Nature* 345: 224–229.
- 455 5. Congleton J, MacDonald R, Yen A (2012) Src inhibitors, PP2 and dasatinib, increase  
456 retinoic acid-induced association of Lyn and c-Raf (S259) and enhance MAPK-  
457 dependent differentiation of myeloid leukemia cells. *Leukemia* 26: 1180-8.
- 458 6. Shen M, Bunaci R, Congleton J, Jensen H, Sayam L, et al. (2011) Interferon regula-  
459 tory factor-1 binds c-Cbl, enhances mitogen activated protein kinase signaling and  
460 promotes retinoic acid-induced differentiation of HL-60 human myelo-monoblastic  
461 leukemia cells. *Leuk Lymphoma* 52: 2372-9.
- 462 7. Shen M, Yen A (2009) c-Cbl tyrosine kinase-binding domain mutant G306E abolishes  
463 the interaction of c-Cbl with CD38 and fails to promote retinoic acid-induced cell dif-  
464 ferentiation and G0 arrest. *J Biol Chem* 284: 25664–25677.
- 465 8. Yen A, Varvayanis S, Smith J, Lamkin T (2006) Retinoic acid induces expression of  
466 SLP-76: expression with c-FMS enhances ERK activation and retinoic acid-induced  
467 differentiation/G0 arrest of HL-60 cells. *Eur J Cell Biol* 85: 117–132.

- 468 9. Marchisio M, Bertagnolo V, Colamussi ML, Capitani S, Neri LM (1998) Phosphatidylinositol 3-kinase in HL-60 nuclei is bound to the nuclear matrix and increases during  
469 granulocytic differentiation. *Biochem Biophys Res Commun* 253: 346-51.
- 470
- 471 10. Congleton J, Jiang H, Malavasi F, Lin H, Yen A (2011) ATRA-induced HL-60 myeloid  
472 leukemia cell differentiation depends on the CD38 cytosolic tail needed for membrane  
473 localization, but CD38 enzymatic activity is unnecessary. *Exp Cell Res* 317: 910–  
474 919.
- 475 11. Wang J, Yen A (2004) A novel retinoic acid-responsive element regulates retinoic acid  
476 induced BLR1 expression. *Mol Cell Biol* 24: 2423 - 2443.
- 477 12. Yen A (1990) HL-60 cells as a model of growth and differentiation: the significance of  
478 variant cells. *Hematology Review* 4: 5-46.
- 479 13. Yang T, Xiong Q, Enslen H, Davis R, Chow CW (2002) Phosphorylation of NFATc4 by  
480 p38 mitogen-activated protein kinases. *Mol Cell Biol* 22: 3892–3904.
- 481 14. Wang J, Yen A (2008) A MAPK-positive Feedback Mechanism for BLR1 Signaling  
482 Propels Retinoic Acid-triggered Differentiation and Cell Cycle Arrest. *J Biol Chem*  
483 283: 4375–4386.
- 484 15. Tasseff R, Nayak S, Song S, Yen A, Varner J (2011) Modeling and analysis of retinoic  
485 acid induced differentiation of uncommitted precursor cells. *Integr Biol* 3: 578 - 591.
- 486 16. Katagiri K, Hattori S, Nakamura S, Yamamoto T, Yoshida T, et al. (1994) Activation  
487 of ras and formation of gap complex during tpa-induced monocytic differentiation of  
488 hl-60 cells. *Blood* 84: 1780–1789.
- 489 17. Miranda MB, Johnson DE (2007) Signal transduction pathways that contribute to  
490 myeloid differentiation. *Leukemia* 21: 1363–1377.
- 491 18. Hickstein DD, Back AL, Collins SJ (1989) Regulation of expression of the cd11b and  
492 cd18 subunits of the neutrophil adherence receptor during human myeloid differenti-  
493 ation. *J Biol Chem* 264: 21812–21817.

- 494 19. Hornstein I, Alcover A, Katzav S (2004) Vav proteins, masters of the world of cy-  
495 toskeleton organization. *Cell Signal* 16: 1-11.
- 496 20. Song JS, Gomez J, Stancato LF, Rivera J (1996) Association of a p95 vav-containing  
497 signaling complex with the fcepsiloniori gamma chain in the rbl-2h3 mast cell line. ev-  
498 idence for a constitutive in vivo association of vav with grb2, raf-1, and erk2 in an  
499 active complex. *J Biol Chem* 271: 26962–26970.
- 500 21. Costello PS, Walters AE, Mee PJ, Turner M, Reynolds LF, et al. (1999) The rho-family  
501 gtp exchange factor vav is a critical transducer of t cell receptor signals to the calcium,  
502 erk, and nf-kappab pathways. *Proc Natl Acad Sci U S A* 96: 3035–3040.
- 503 22. Graham D, Robertson C, Bautista J, Mascarenhas F, Diacovo M, et al. (2007)  
504 Neutrophil-mediated oxidative burst and host defense are controlled by a Vav-  
505 PLCgamma2 signaling axis in mice. *J Clin Invest* 117: 3445–3452.
- 506 23. Cleghon V, Morrison DK (1994) Raf-1 interacts with fyn and src in a non-  
507 phosphotyrosine-dependent manner. *J Biol Chem* 269: 17749–17755.
- 508 24. Zimmermann S, Moelling K (1999) Phosphorylation and regulation of raf by akt (pro-  
509 tein kinase b). *Science* 286: 1741–1744.
- 510 25. Ritt DA, Zhou M, Conrads TP, Veenstra TD, Copeland TD, et al. (2007) Ck2 is a  
511 component of the ksr1 scaffold complex that contributes to raf kinase activation. *Curr*  
512 *Biol* 17: 179–184.
- 513 26. Hekman M, Wiese S, Metz R, Albert S, Troppmair J, et al. (2004) Dynamic changes in  
514 c-raf phosphorylation and 14-3-3 protein binding in response to growth factor stimula-  
515 tion: differential roles of 14-3-3 protein binding sites. *J Biol Chem* 279: 14074–14086.
- 516 27. Dhillon AS, Yip YY, Grindlay GJ, Pakay JL, Dangers M, et al. (2009) The c-terminus  
517 of raf-1 acts as a 14-3-3-dependent activation switch. *Cell Signal* 21: 1645–1651.
- 518 28. Kim HS, Lim IK (2009) Phosphorylated extracellular signal-regulated protein kinases  
519 1 and 2 phosphorylate sp1 on serine 59 and regulate cellular senescence via tran-

- 520 scription of p21sdi1/cip1/waf1. *J Biol Chem* 284: 15475–15486.
- 521 29. Milanini-Mongiat J, Pouyss?gur J, Pag?o G (2002) Identification of two sp1 phospho-  
522 rylation sites for p42/p44 mitogen-activated protein kinases: their implication in vas-  
523 cular endothelial growth factor gene transcription. *J Biol Chem* 277: 20631–20639.
- 524 30. Zhang Y, Cho YY, Petersen BL, Zhu F, Dong Z (2004) Evidence of stat1 phosphory-  
525 lation modulated by mapks, mek1 and msk1. *Carcinogenesis* 25: 1165–1175.
- 526 31. Li Z, Theus MH, Wei L (2006) Role of erk 1/2 signaling in neuronal differentiation of  
527 cultured embryonic stem cells. *Dev Growth Differ* 48: 513–523.
- 528 32. Yen A, Reece SL, Albright KL (1984) Dependence of hl-60 myeloid cell differentiation  
529 on continuous and split retinoic acid exposures: precommitment memory associated  
530 with altered nuclear structure. *J Cell Physiol* 118: 277–286.
- 531 33. Ferrell J (2002) Self-perpetuating states in signal transduction: positive feedback,  
532 double-negative feedback and bistability. *Curr Opin Cell Biol* 14: 140-8.
- 533 34. Xiong W, Ferrell J (2003) A positive-feedback-based bistable 'memory module' that  
534 governs a cell fate decision. *Nature* 426: 460-5.
- 535 35. Bagci EZ, Vodovotz Y, Billiar TR, Ermentrout GB, Bahar I (2006) Bistability in apop-  
536 tosis: roles of bax, bcl-2, and mitochondrial permeability transition pores. *Biophys J*  
537 90: 1546-59.
- 538 36. Luan D, Zai M, Varner JD (2007) Computationally derived points of fragility of a human  
539 cascade are consistent with current therapeutic strategies. *PLoS Comput Biol* 3:  
540 e142.
- 541 37. Wayman JA, Sagar A, Varner JD (2015) Dynamic modeling of cell-free biochemical  
542 networks using effective kinetic models. *Processes* 3: 138.
- 543 38. Milo R, Jorgensen P, Moran U, Weber G, Springer M (2010) Bionumbers—the  
544 database of key numbers in molecular and cell biology. *Nucleic Acids Res* 38: D750-  
545 3.

- 546 39. Bezanson J, Edelman A, Karpinski S, Shah VB (2014) Julia: A fresh approach to  
547 numerical computing. CoRR abs/1411.1607.
- 548 40. Hindmarsh A, Brown P, Grant K, Lee S, Serban R, et al. (2005) Sundials: Suite of non-  
549 linear and differential/algebraic equation solvers. ACM Transactions on Mathematical  
550 Software 31: 363-396.
- 551 41. Brooks SC, Kazmer S, Levin AA, Yen A (1996) Myeloid differentiation and retinoblas-  
552 toma phosphorylation changes in HL-60 cells induced by retinoic acid receptor- and  
553 retinoid X receptor-selective retinoic acid analogs. Blood 87: 227–237.
- 554 42. Jensen HA, Yourish HB, Bunaciu RP, Varner JD, Yen A (2015) Induced myelomono-  
555 cytic differentiation in leukemia cells is accompanied by noncanonical transcription  
556 factor expression. FEBS Open Bio 5: 789-800.

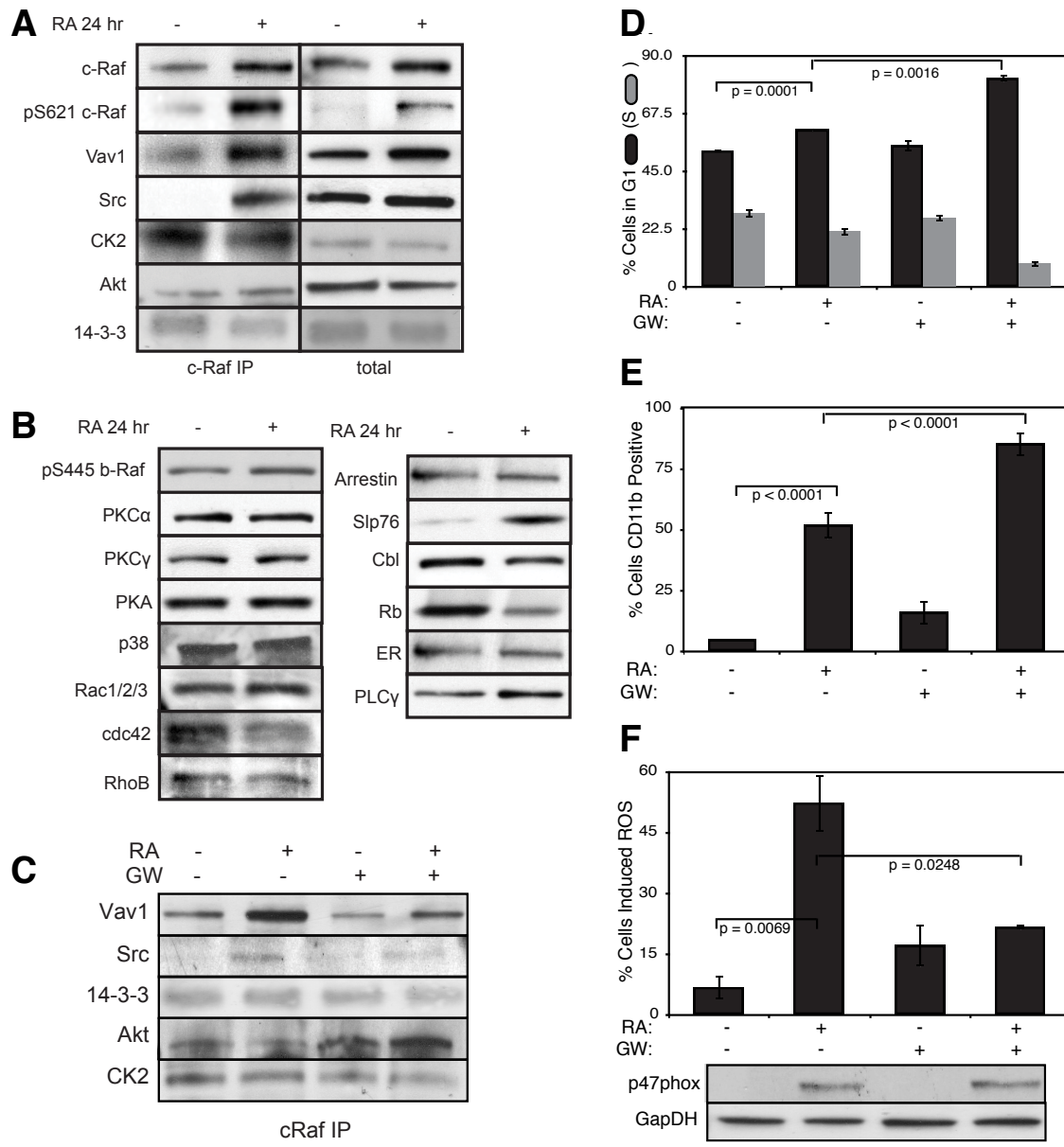


**Fig. 1:** Investigation of a panel of possible Raf interaction partners in the presence and absence of ATRA. A: Species identified to precipitate out with Raf: first column shows Western blot analysis on total Raf immunoprecipitation with and without 24 hr ATRA treatment and the second on total lysate. B: The expression of species considered that did not precipitate out with Raf at levels detectable by Western blot analysis on total lysate. C: Effect of the Raf inhibitor GW5074 on Raf interactions as determined by Western blot analysis of total Raf immunoprecipitation. The Authors note the signal associated with Src was found to be weak. D: Cell Cycle distribution as determined by flow cytometry indicated arrest induced by ATRA, which was increased by the addition of GW5074. E: Expression of the cell surface marker CD11b as determined by flow cytometry indicated increased expression induced by ATRA, which was enhanced by the addition of GW5074. F: Inducible reactive oxygen species (ROS) as determined by DCF flow cytometry. The functional differentiation response of ATRA treated cells was mitigated by GW5074.

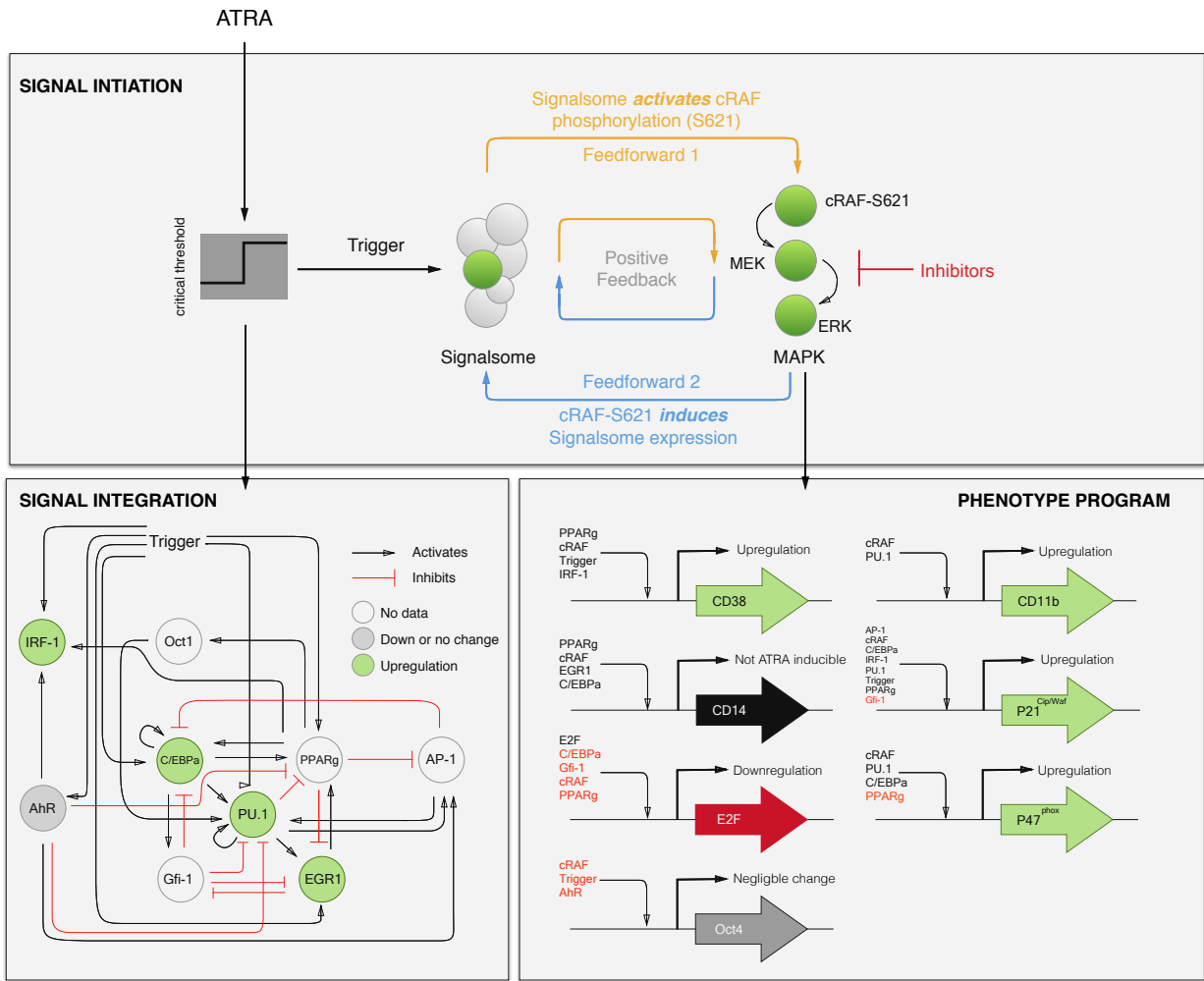


**Fig. 2:** Schematic of the effective ATRA differentiation circuit. Above a critical threshold, ATRA activates an upstream Trigger, which induces signalsome complex formation. Signalsome activates the mitogen-activated protein kinase (MAPK) cascade which in turn drives the differentiation program and signalsome formation. Both Trigger and activated cRAF-S621 drive a phenotype gene expression program responsible for differentiation. Trigger activates the expression of a series of transcription factors which in combination with cRAF-S621 result in phenotypic change.

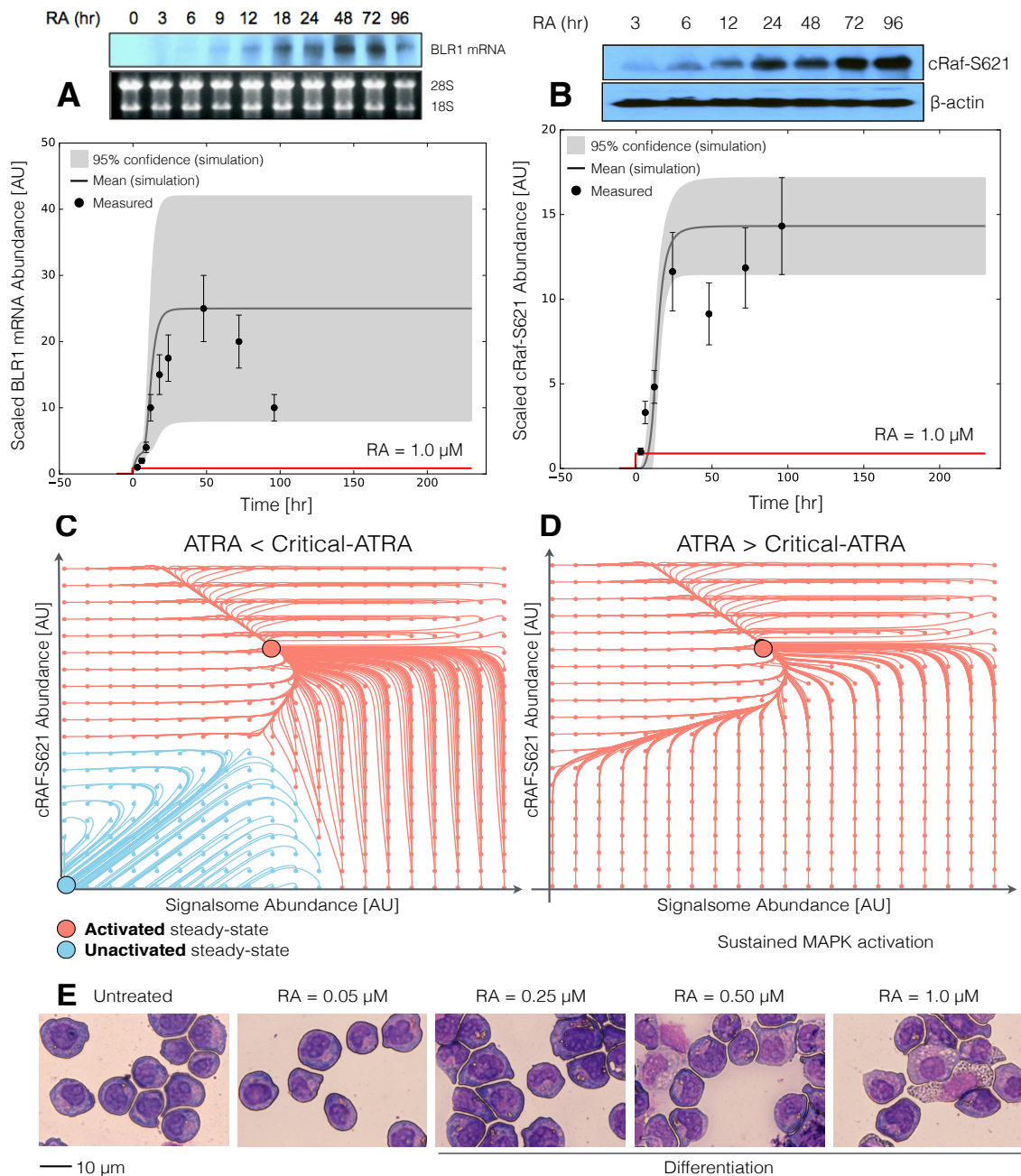


**Fig. 3:** Model analysis for ATRA-induced HL-60 differentiation. A: BLR1 mRNA versus time following exposure to  $1\mu\text{M}$  ATRA at  $t = 0$  hr. B: cRAF-pS621 versus time following exposure to  $1\mu\text{M}$  ATRA at  $t = 0$  hr. Points denote experimental measurements, solid lines denote the mean model performance. Shaded regions denote the 99% confidence interval calculated over the parameter ensemble. C: Signalsome and cRAF-pS621 nullclines for ATRA below the critical threshold. The model had two stable steady states and a single unstable state in this regime. D: Signalsome and cRAF-pS621 nullclines for ATRA above the critical threshold. In this regime the model had only a single stable steady state. E: Morphology of HL-60 as a function of ATRA concentration ( $t = 72$  hr).

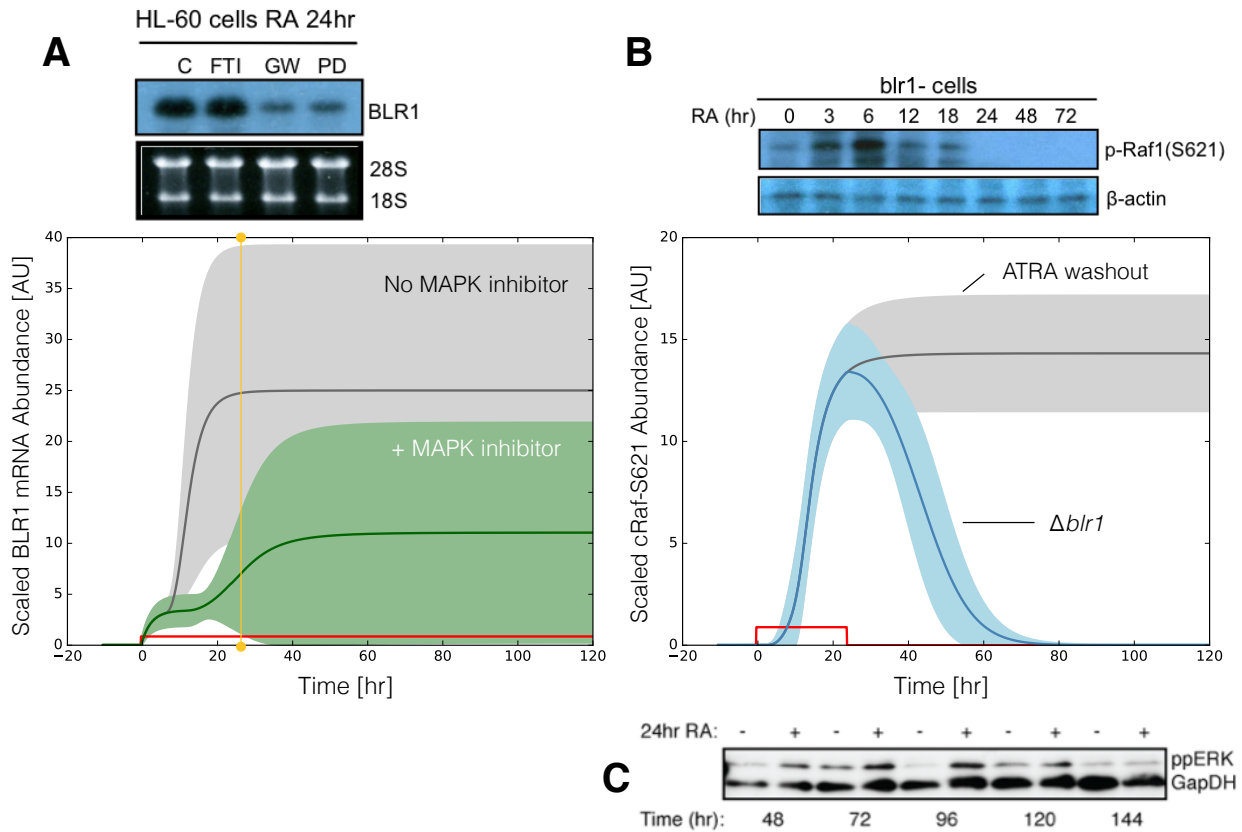


**Fig. 4:** Model simulation following exposure to  $1\mu\text{M}$  ATRA. A: BLR1 mRNA versus time with and without MAPK inhibitor. B: cRAF-pS621 versus time following pulsed exposure to  $1\mu\text{M}$  ATRA with and without BLR1. Solid lines denote the mean model performance, while shaded regions denote the 99% confidence interval calculated over the parameter ensemble. C: Western blot analysis of phosphorylated ERK1/2 in ATRA washout experiments. Experimental data in panels A and B were reproduced from Wang and Yen (14), data in panel C is reported in this study.

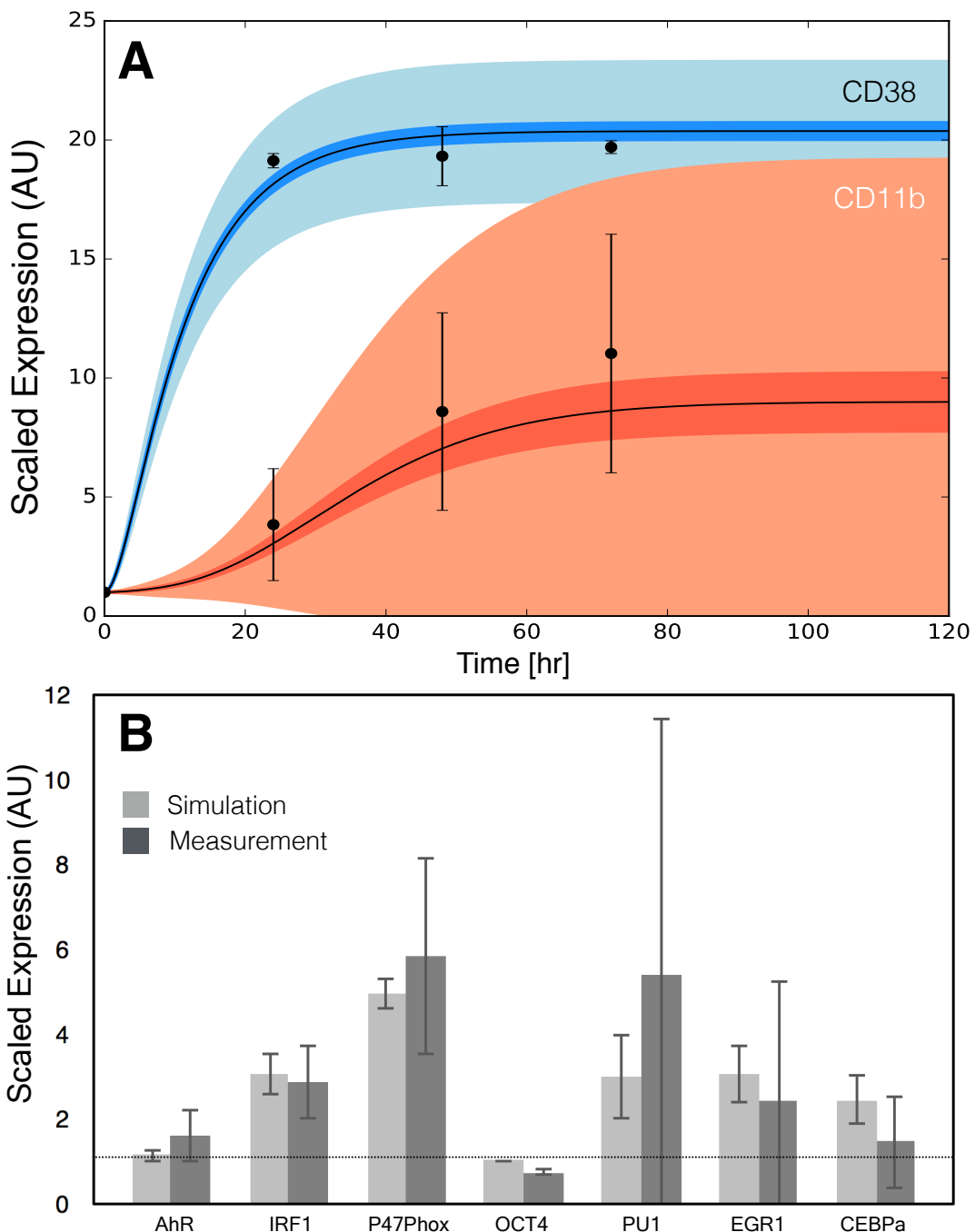


**Fig. 5:** Model simulation of the HL-60 gene expression program following exposure to  $1\mu\text{M}$  ATRA at  $t = 0$  hr. A: CD38 and CD11b expression versus time following ATRA exposure at time  $t = 0$  hr. B: Gene expression at  $t = 48$  hr following ATRA exposure. Experimental data in panels A and B were reproduced from Jensen et al. (42).